Applied Physics Letters

High-kinetic inductance additive manufactured superconducting microwave cavity

Cite as: Appl. Phys. Lett. **111**, 202602 (2017); https://doi.org/10.1063/1.5000241
Submitted: 14 August 2017 • Accepted: 24 October 2017 • Published Online: 13 November 2017

Eric T. Holland, Yaniv J. Rosen, Nicholas Materise, et al.

openaccess
View Online
Export Citation
CrossMark

ARTICLES YOU MAY BE INTERESTED IN

A quantum engineer's guide to superconducting qubits
Applied Physics Reviews **6**, 021318 (2019); https://doi.org/10.1063/1.5089550

Materials loss measurements using superconducting microwave resonators
Review of Scientific Instruments **91**, 091101 (2020); https://doi.org/10.1063/5.0017378

Surface participation and dielectric loss in superconducting qubits
Applied Physics Letters **107**, 162601 (2015); https://doi.org/10.1063/1.4934486

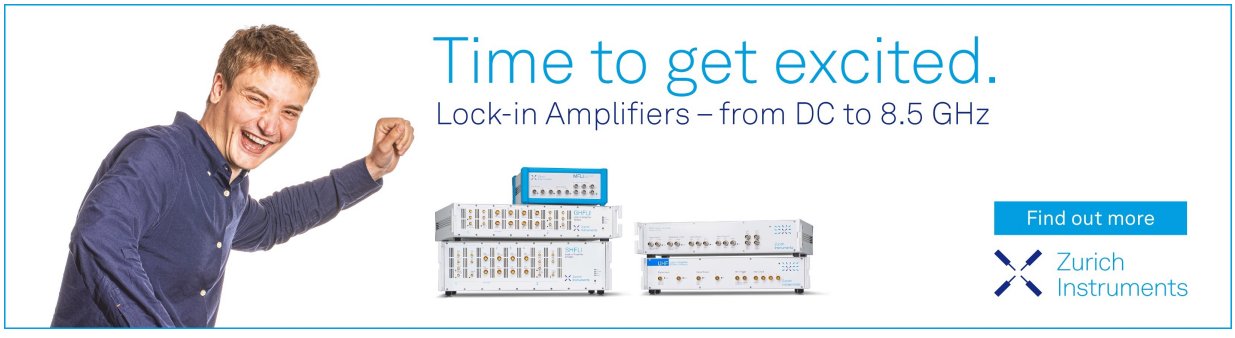

© 2017 Author(s).

AIP Publishing

High-kinetic inductance additive manufactured superconducting microwave cavity

Eric T. Holland,[1,a)] Yaniv J. Rosen,[1] Nicholas Materise,[1] Nathan Woollett,[1] Thomas Voisin,[1] Y. Morris Wang,[1] Sharon G. Torres,[1] Jorge Mireles,[2] Gianpaolo Carosi,[1] and Jonathan L DuBois[1]
[1]*Lawrence Livermore National Laboratory, Livermore, California 94550, USA*
[2]*The University of Texas at El Paso, W.M. Keck Center, El Paso, Texas 79968, USA*

(Received 14 August 2017; accepted 24 October 2017; published online 13 November 2017)

Investigations into the microwave surface impedance of superconducting resonators have led to the development of single photon counters that rely on kinetic inductance for their operation, while concurrent progress in additive manufacturing, "3D printing," opens up a previously inaccessible design space for waveguide resonators. In this manuscript, we present results from the synthesis of these two technologies in a titanium, aluminum, vanadium (Ti-6Al-4V) superconducting radio frequency resonator which exploits a design unattainable through conventional fabrication means. We find that Ti-6Al-4V has two distinct superconducting transition temperatures observable in heat capacity measurements. The higher transition temperature is in agreement with DC resistance measurements, while the lower transition temperature, not previously known in the literature, is consistent with the observed temperature dependence of the superconducting microwave surface impedance. From the surface reactance, we extract a London penetration depth of $8 \pm 3\,\mu$m—roughly an order of magnitude larger than other titanium alloys and several orders of magnitude larger than other conventional elemental superconductors. *© 2017 Author(s). All article content, except where otherwise noted, is licensed under a Creative Commons Attribution (CC BY) license (http://creativecommons.org/licenses/by/4.0/).* https://doi.org/10.1063/1.5000241

The Landau-Ginzburg model for superconductivity is a mean field theory that parametrizes the superconducting condensate with two key length scales.[1,2] The first length scale is the Pippard coherence length, ζ, which is the average distance between Cooper pairs in the condensate. The second length scale, the London penetration depth, λ, describes the distance over which a magnetic field penetrates into a superconductor. The ratio between the Pippard coherence length and the London penetration depth is commonly used to characterize whether a superconductor is type I ($\zeta/\lambda > \sqrt{\frac{1}{2}}$), field expelling, or type II ($\zeta/\lambda < \sqrt{\frac{1}{2}}$), field penetrating material.[3] As such, precise measurements of either the Pippard coherence length or, as in the case of this manuscript, the London penetration depth are critical for the accurate description of the superconducting material.

In superconducting radio frequency resonators, the London penetration depth describes the distance over which energy is stored in the motion of Cooper pairs. This energy storage mechanism is associated with a current and therefore described as a kinetic inductance. Kinetic inductance is determined, in part, by the equilibrium temperature in relation to the superconducting transition temperature. This feature of kinetic inductance has been exploited in a number of applications including radiation detectors with up to single photon resolution by the so-called microwave kinetic inductance detectors (MKIDs).[4]

In this letter, we show that titanium, aluminum, vanadium, Ti-6Al-4V, (90% Ti, 6% Al, and 4% V by weight) is a high kinetic inductance superconductor, that the hexagonal close packed (alpha) phase is indeed a superconductor contrary to suspicion in the previous literature,[5] and that additive manufacturing (AM) enables a parameter space of seamless resonator designs left unexplored in previous work.[6] We investigate the superconducting properties of bulk AM Ti-6Al-4V by measurements of the DC resistance, heat capacity, and microwave surface impedance. Thus, a main result of this manuscript is a measurement of the London penetration depth for the most widely used titanium alloy in industry.[5]

Titanium alloys, and Ti-6Al-4V in particular, are commonly used in AM processes (see Refs. 8–10 for examples). In the present work, we have employed a selective laser melting (SLM) process[11] to fabricate our samples. SLM works by using a high powered laser to melt and solidify a metallic powder according to a digitally designed geometry. The laser power and rastering parameters used to fabricate the resonator structures under study were optimized for mechanical performance and minimal porosity.[12] In addition, our samples received a post-processing heat treatment designed for selecting the bulk microstructure. The heat treatment involved a half hour duration heat ramp to 900 °C in atmosphere, which was maintained for an hour, and finally quench cooled to room temperature with argon gas.

We begin our characterization of Ti-6Al-4V by investigating the bulk microstructure and elemental composition to compare the AM sample to bulk Ti-6Al-4V. To investigate the bulk microstructure, we performed a cross sectional cut on the sample after performing characterization of the superconducting microwave surface impedance presented later in this work. After the cross section, the sample received an

a)holland25@llnl.gov

 © Author(s) 2017.

acid etch (immersed in 10 ml HF, 5 ml HNO_3, and 85 ml H_2O for 15 s) to reliably produce contrast between the α and β phases. After acid etch, shown in Fig. 1(d) is a representative optical microscopy image from our sample. Qualitatively, the surface microstructure is as expected—specifically, the sample is dense and has the expected microstructure [Fig. 1(b)]. In Fig. 1(c), the results of energy-dispersive X-ray spectroscopy (EDS) demonstrate an elemental composition of titanium (90%), aluminum (6%), vanadium (4%) and a less then percent contribution from other impurities such as iron. Further localized EDS and SEM studies in the interior and near the sample surface were consistent with those shown with no evidence for spatial inhomogeneities in the phase, crystal structure, or composition. We therefore conclude that our samples are qualitatively equivalent to bulk Ti-6Al-4V, which has undergone a similar heat treatment during cooling, and that the results presented in this manuscript are not limited to AM Ti-6Al-4V.

Through previous DC resistance measurements, it is known that Ti-6Al-4V is a superconductor with a single transition temperature that varies in the range of 1.3 K–6.3 K depending on oxidation treatment and post-processing annealing.[13–19] In agreement with this literature, we observe a bulk material superconducting transition temperature of 4.5 K (Fig. 2, solid green triangles, 90% drop value) through a four point measurement in a Quantum Design Physical

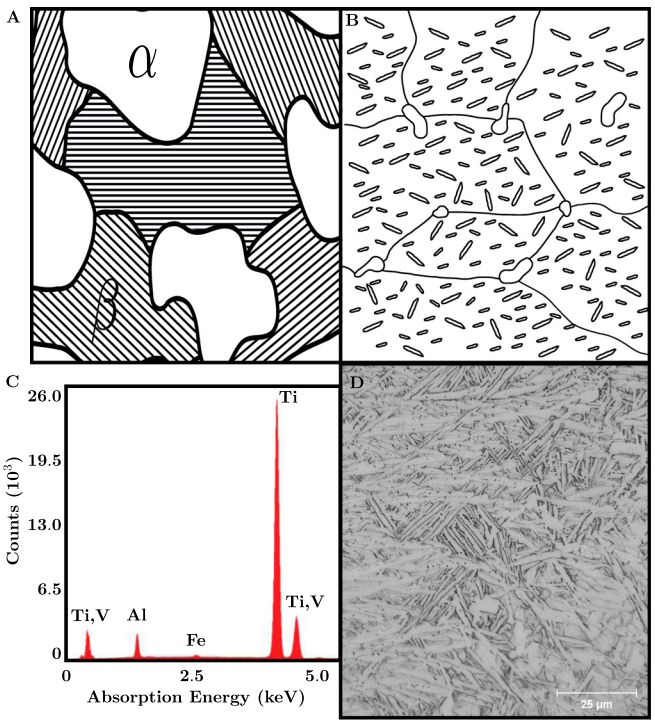

FIG. 1. Ti-6Al-4V microstructure and elemental composition. (a) Nominal sketch of the typical bulk microstructure of Ti-6Al-4V before temperature anneal (see Ref. 7 for more details on the Ti-6Al-4V microstructure). White regions depict the hexagonal close packed, α phase. Repeating line regions are body centered cubic, β phase. (b) Sketch of the idealized microstructure of Ti-6Al-4V for optimal mechanical performance post high temperature anneal. Now, white regions represent the α phase dispersed within martensitic β phase regions. (c) Representative energy dispersive X-ray spectroscopy of the Ti-6Al-4V surface composition after acid etch. Titanium (90%), aluminum (6%), vanadium (4%), and iron (<0.5%) are all in percentages as used commercially for bulk Ti-6Al-4V. (d) Optical microscopy image of the Ti-6Al-4V microstructure after optimized acid etch.

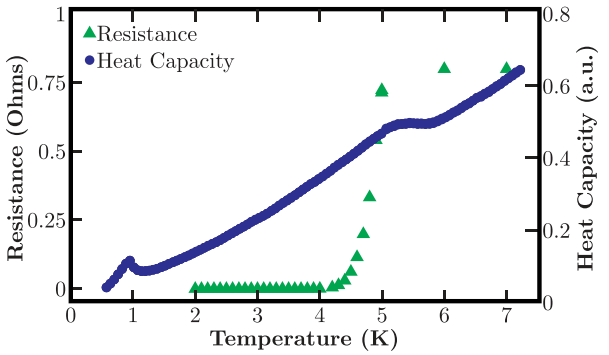

FIG. 2. DC resistance and heat capacity. The DC resistance (left y-axis) plotted as a function of equilibrium temperature (green triangles) of a four point measurement performed in a quantum design physical property measurement system shows a superconducting transition temperature of 4.5 K. The heat capacity (right y-axis) plotted as a function of equilibrium temperature (blue dots) displays two distinct superconducting phase transitions. The lower transition temperature, 0.95 K, is not observed in the DC resistance measurements presumably because it is shorted out by other superconducting pathways.

Property Measurement System. However, by investigating the low temperature behavior of the bulk heat capacity for Ti-6Al-4V, we observe two superconducting phase transitions as shown in Fig. 2 (blue dots). The first phase transition at higher temperatures is in qualitative agreement with our DC measurements. The second phase transition is observed at a much lower temperature of 0.95 K. Additionally, the lower transition temperature is missing from the literature. The theoretical predictions of a multicomponent superconducting gap were made in 1959 by Suhl *et al.*,[20] and a broad overview of multicomponent superconductivity can be found in Ref. 21 and references within.

From the above characterization, we learn that AM Ti-6Al-4V may be a robust material to fabricate superconducting resonators and proceed to characterize its superconducting microwave surface impedance in the quantum regime (i.e., $\hbar\omega < k_bT$, and the average photon number in the resonator is $\bar{n} \approx 1$). The results presented in this work are part of an ongoing study investigating the role of geometric effects on resonator performance. In designing the resonator structure for this study, we employed the expanded design space offered by AM fabrication to explore the relative importance of loss mechanisms arising from inductive (surface resistance) and capacitive (dielectric loss tangent) contributions. The resonator under study in this work (see Fig. 3) is a variant of a well-performing aluminum coaxial quarter wave resonator with millisecond lifetimes in the quantum regime[22,23] designed to minimize the surface current density on resonance.

Characterization of the superconducting microwave surface impedance was performed using a Janis model JD-250 (wet) He3-He4 dilution refrigeration system. Cryogenic attenuations of 40 dB are included on the 1 K pot stage and 20 dB on the mixing chamber stage (20 mK base temperature) to filter the black body noise power down to the that of the mixing chamber. The Ti-6Al-4V conical resonator and a gold plated copper box containing planar aluminum coplanar waveguide resonators were multiplexed on a high purity oxygen free copper cold finger attached to the mixing chamber. For multiplexing, we used a resistive power dividing SMA T attached to an SMA connector with post that couples

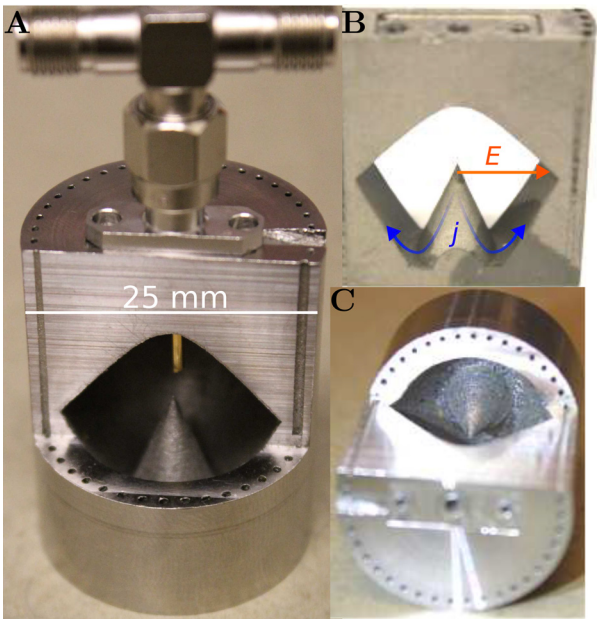

FIG. 3. AM Ti-6Al-4V conical resonator. (a) A nominally identical cavity is cut to reveal the internal structure. A resistive SMA T is connected to an SMA connector which is evanescently coupled to the resonant mode of the conical resonator. (b) Cross-sectional cut of the Ti-6Al-4V resonator after an acid etch. On resonance, the current flows along the base of the cone and in the walls, while the electric field is maximal at the tip of the cone. (c) Alternative angle, with the SMA connector removed, of the conical resonator, showing the internal geometry and coupling mechanism.

below cutoff through a cylindrical waveguide (evanescently) to the conical resonator similar to work done in Ref. 24. The samples were fully enclosed in an Amuneal A4K magnetic shield attenuating the ambient magnetic field to less than a milliGauss. The magnetic shielding is thermally heat sunk to a light tight copper shield blocking stray infrared radiation. The output of our samples led into two 4–8 GHz PAMTECH model CTH0408KI isolators in series, providing reverse isolation in excess of 40 dB, allowing investigations of the resonators in the quantum regime. An output SMA line of superconducting NbTiN led to the cryogenic HEMT amplifier at the 1 K pot stage (Low Noise Factory model `LNF_LNC_4_8C`), offering 40 dB of gain and roughly 2 K of added noise. At room temperature, the signal is sent through another amplifier (MITEQ AMF-5D-00101200-23-10P-LPN), offering another 40 dB of gain. All measurements were performed with a Keysight PNA vector network analyzer model N5230C.

The resonance of the conical Ti-6Al-4V sample at 20 mK was found to be $\omega_0/2\pi = 7.50$ GHz, in agreement with simulation. To study the temperature dependence of the superconducting microwave surface impedance, we varied the applied heat delivered to the mixing chamber of our dilution refrigerator. At each temperature, the samples were allowed to equilibrate for two hours before measurements were taken. This time scale was determined by a series of overnight runs at fixed temperatures of 475 mK and 500 mK to determine the time constant for the measured $|S_{21}|^2$ to have only Gaussian noise about a fixed mean and no systematic variation. All fits to the measured $|S_{21}|^2$ response from the vector network analyzer were performed using a complex coupling quality factor, a resonance frequency, and an internal quality factor as in Ref. 25.

The temperature dependence of the fractional frequency shift ($\frac{\delta f}{f}$) can be related in a straightforward way to the surface reactance of the resonator.[26] In Fig. 4, the fractional frequency shift (green triangles, left y-axis) is plotted as a function of equilibrium temperature recorded on the mixing chamber. Along with the results for the Ti-6Al-4V resonator, we show frequency shift results for a simultaneously measured planar aluminum resonator (identical to Ref. 27). All points in the figure represent the average of three measurements of $|S_{21}|^2$, and the size of the points is substantially larger than the associated error bars. The fractional frequency shift temperature dependence is well fit by a simple two fluid model[28]

$$\frac{\delta f(T)}{f} = \frac{-\alpha_{KI}}{2\left(1-\left(\frac{T}{T_c}\right)^4\right)} + \frac{\alpha_{KI}}{2}, \tag{1}$$

where α_{KI} is the zero temperature kinetic inductance fraction and T_c is the superconducting transition temperature. From this fit, we extract a kinetic inductance fraction of $\alpha_{KI} = 4 \times 10^{--3} \pm 2 \times 10^{--3}$ and $T_c = 0.95 \pm 0.1$ K. We note that this fitted value is consistent with the lower transition temperature observed in the heat capacity measurements from Fig. 2.

We relate the extracted kinetic inductance fraction of the resonator to the zero temperature London penetration depth, λ_0, via the magnetic field, H, and participation ratio, p_{mag} as[24]

$$\alpha_{KI} = \lambda_0 p_{mag} = \lambda_0 \frac{\int H^2 dA}{\int H^2 dV}. \tag{2}$$

Evaluation of (2) requires a calculation of the magnetic field energy stored on the surface, $\int H^2 dA$, compared to the magnetic field energy stored in the volume, $\int H^2 dV$. This can be

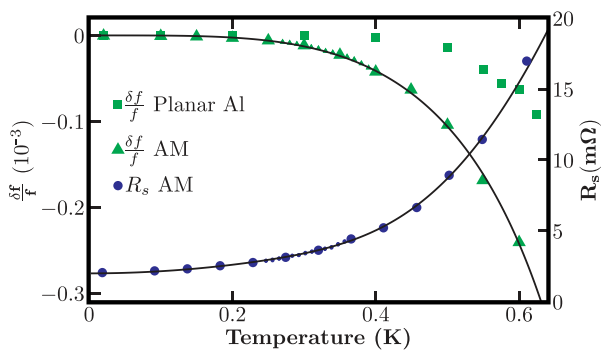

FIG. 4. Temperature dependence of the superconducting microwave surface impedance. Green triangles (small triangles are finer resolution data in this temperature region) show the fractional frequency shift of the Ti-6Al-4V conical resonator as a function of equilibrium temperature. Shown on the same scale for reference is the fractional frequency shift as a function of temperature (green squares with smaller squares being finer resolution data in this temperature region) of a coplanar waveguide aluminum resonator. Blue dots show the resistance of the Ti-6Al-4V resonator as a function of temperature.

trivially calculated in an electrodynamic solver such as ANSYS HFSS or COMSOL. For this manuscript, both software suites were used and agreed upon a value of $537\,\mathrm{m}^{-1}$ for the conical geometry with a relative uncertainty of 1% when accounting for numerical inaccuracies and machining tolerances. This is well within a factor of two of what one can calculate via closed form analytic solutions of a conventional coaxial geometry. Using this value of the magnetic participation ratio, we extract $\lambda_0 = 8 \pm 3\,\mu\mathrm{m}$. This length scale is quite large when compared with aluminum (52 nm),[24] niobium (32 nm),[28] or even titanium nitride (575 nm).[29] We note that although this manuscript focuses on the results of a single conical cavity, we find consistent kinetic inductance performance in other more conventional coaxial cavity designs ($\lambda_0 = 15 \pm 10\,\mu\mathrm{m}$) whose description is outside the scope of this manuscript. Specifically, these results are reproducible across different resonator designs, and we conclude our findings to be an intrinsic property of Ti-6Al-4V. Therefore, Ti-6Al-4V stores a tremendous amount of energy in the motion of the Cooper pairs as compared to other commonly used superconductors in microwave applications.

Finally, we investigate the resistive part of the superconducting microwave surface impedance by transforming the extracted internal quality factor ($Q_i \approx 3 \times 10^4$ in the quantum regime). This is accomplished by relating the measured internal quality factor at various temperatures, $Q_i(T)$, to the temperature dependent surface resistance, $R_s(T)$, through the magnetic participation ratio, the permeability of free space, μ_0, and the resonance frequency in angular units, ω_0, as[30]

$$R_s(T) = \frac{\mu_0 \omega_0}{p_{mag} Q_i(T)}. \tag{3}$$

In Fig. 4, on the right in blue dots, we plot the surface resistance as a function of equilibrium temperature on the mixing chamber. We fit the measured surface resistance with a functional form that is comprised of a BCS component (exponential), a metallic, Fermi liquid, component (quadratic), and a residual resistance (constant)

$$R_s(T) = \frac{A}{T} \exp\left(-\frac{\Delta_0}{k_b T}\right) + BT^2 + R_0. \tag{4}$$

At high temperatures, the dominant contribution to the surface resistance is from quasiparticle loss (exponential) and the superconducting gap (Δ_0) is consistent with the fractional frequency shift. However, at lower temperatures, the temperature dependence is dominated by a T^2 behavior consistent with a classical Fermi fluid contribution.[31] Power dependent measurements of this resonator displayed no appreciable power dependence in the internal quality factor, indicating that dissipation due to low energy defects was not a dominant source of loss in this system.[26] Given the explicit T^2 dependence at low temperature and the lack of a strong power dependence, we attribute the low temperature residual resistance to conductive losses in the normal metal part of the microwave surface impedance.

In conclusion, we present a measurement of the London penetration length of one of the most abundant titanium alloys (Ti-6Al-4V) of $8 \pm 3\,\mu\mathrm{m}$. Through careful temperature dependence studies, we extract the effective transition temperature governing the surface impedance at microwave frequencies to find a superconducting gap consistent with heat capacity measurements of the same sample. Unique to this work, we demonstrate proof of principle additive manufacturing based fabrication and geometry optimization of superconducting resonators which could not be constructed out of one contiguous piece by conventional fabrication techniques. Finally, this work demonstrates that Ti-6Al-4V is a high kinetic inductance material.

We would like to thank Scott McCall for assistance with the PPMS system, Will Oliver for providing the aluminum planar resonators, and Sean Durham and Jesse Hamblen for solving all our problems. This work was performed under the auspices of the U.S. Department of Energy by the Lawrence Livermore National Laboratory under Contract No. DE-AC52-07NA27344. This work was supported by the Laboratory Directed Research and Development under Grant No. 16-SI-004. LLNL-JRNL-733239.

[1]L. D. Landau and V. Ginzburg, Zh. Eksp. Teor. Fiz. **20**, 1064 (1950).
[2]L. P. Gor'kov, Sov. Phys. JETP **9**, 1364 (1959).
[3]M. Tinkham, *Introduction to Superconductivity* (Courier Corporation, 1996).
[4]P. K. Day, H. G. LeDuc, B. A. Mazin, A. Vayonakis, and J. Zmuidzinas, Nature **425**, 817 (2003).
[5]C. Leyens and M. Peters, *Titanium and Titanium Alloys: Fundamentals and Applications* (John Wiley & Sons, 2003).
[6]D. L. Creedon, M. Goryachev, N. Kostylev, T. B. Sercombe, and M. E. Tobar, Appl. Phys. Lett. **109**, 032601 (2016).
[7]M. D. Gorman, A. P. Woodfield, and B. A. Link, "Heat treatment for improved properties of alpha-beta titanium-base alloys," U.S. patent 6,284,070 (4 September 2001).
[8]P. Kobryn and S. Semiatin, JOM **53**, 40 (2001).
[9]L. Thijs, F. Verhaeghe, T. Craeghs, J. Van Humbeeck, and J.-P. Kruth, Acta Mater. **58**, 3303 (2010).
[10]G. Pyka, A. Burakowski, G. Kerckhofs, M. Moesen, S. Van Bael, J. Schrooten, and M. Wevers, Adv. Eng. Mater. **14**, 363 (2012).
[11]J.-P. Kruth, G. Levy, F. Klocke, and T. Childs, CIRP Ann.-Manuf. Technol. **56**, 730 (2007).
[12]M. J. Matthews, G. Guss, S. A. Khairallah, A. M. Rubenchik, P. J. Depond, and W. E. King, Acta Mater. **114**, 33 (2016).
[13]A. Clark, G. Childs, and G. Wallace, Cryogenics **10**, 295 (1970).
[14]R. Lepper, E. G. Wolff, and G. J. Mills, "Ac permeability studies of ternary alloys at cryogenic temperatures," Technical Report No. 4469376 (Northrop Corp., Hawthorne, CA, 1972).
[15]E. Wolff, R. Lepper, and G. Mills, Titanium Sci. Technol. **2**, 843 (1973).
[16]O. Umezawa and K. Ishikawa, Cryogenics **32**, 873 (1992).
[17]U. Divakar, S. Henry, H. Kraus, and A. Tolhurst, Supercond. Sci. Technol. **21**, 065021 (2008).
[18]U. Divakar, S. Henry, H. Kraus, and A. Tolhurst, Supercond. Sci. Technol. **23**, 129801 (2010).
[19]F. Ridgeon, M. Raine, D. Halliday, M. Lakrimi, A. Thomas, and D. Hampshire, IEEE Trans. Appl. Supercond. **27**, 4201205 (2016).
[20]H. Suhl, B. Matthias, and L. Walker, Phys. Rev. Lett. **3**, 552 (1959).
[21]M. V. Milošević, A. Perali, N. Shinohara, K. Tokiwa, H. Fujihisa, Y. Gotoh, S. Ishida, K. Kihou, C. Lee, H. Eisaki *et al.*, Supercond. Sci. Technol. **28**, 60201 (2015).
[22]M. Reagor, W. Pfaff, C. Axline, R. W. Heeres, N. Ofek, K. Sliwa, E. T. Holland, C. Wang, J. Blumoff, K. Chou *et al.*, Phys. Rev. B **94**, 014506 (2016).
[23]C. Wang, Y. Y. Gao, P. Reinhold, R. Heeres, N. Ofek, K. Chou, C. Axline, M. Reagor, J. Blumoff, K. Sliwa *et al.*, Science **352**, 1087 (2016).
[24]M. J. Reagor, H. Paik, G. Catelani, L. Sun, C. Axline, E. T. Holland, I. M. Pop, N. A. Masluk, T. Brecht, L. Frunzio *et al.*, Appl. Phys. Lett. **102**, 192604 (2013).
[25]K. Geerlings, S. Shankar, E. Edwards, L. Frunzio, R. Schoelkopf, and M. Devoret, Appl. Phys. Lett. **100**, 192601 (2012).

[26]J. Gao, M. Daal, A. Vayonakis, S. Kumar, J. Zmuidzinas, B. Sadoulet, B. A. Mazin, P. K. Day, and H. G. Leduc, Appl. Phys. Lett. **92**, 152505 (2008).
[27]J. M. Sage, V. Bolkhovsky, W. D. Oliver, B. Turek, and P. B. Welander, J. Appl. Phys. **109**, 063915 (2011).
[28]J. Turneaure, J. Halbritter, and H. Schwettman, J. Supercond. **4**, 341 (1991).
[29]M. R. Vissers, J. Gao, D. S. Wisbey, D. A. Hite, C. C. Tsuei, A. D. Corcoles, M. Steffen, and D. P. Pappas, Appl. Phys. Lett. **97**, 232509 (2010).
[30]H. Padamsee, Supercond. Sci. Technol. **14**, R28 (2001).
[31]G. Grimvall, *The Electron-Phonon Interaction in Metals* (North Holland, Amsterdam, 1981), Vol. 8.